ISSN (Print) 1226-1750
ISSN (Online) 2233-6656
Journal of Magnetics 28(3), 239-244 (2023) https://doi.org/10.4283/JMAG.2023.28.3.239

Effect of Heat-treatment Temperature on the Formation of ε-Fe_2O_3 Nanoparticles Encapsulated by SiO_2

Trinh Nguyen Thi[1†], Phuoc Cao Van[1†], Kirakosyan Artavazd[1], Chanyong Hwang[2], Jihoon Choi[1], Hyojin Kim[1*], and Jong-Ryul Jeong[1*]

[1]*Department of Material Science and Engineering, Chungnam National University, Daejeon 34134, Republic of Korea*
[2]*Quantum Technology Institute, Korea Research Institute of Standards and Science, Daejeon 34113, Republic of Korea*

(Received 3 February 2023, Received in final form 22 April 2023, Accepted 31 May 2023)

ε-Fe_2O_3 has received attention with particular interest because of its large coercive field at room temperature, high-frequency millimeter-wave absorption, and the coupling of its magnetic and dielectric properties. This work investigated the effect of heat treatment on the formation of ε-Fe_2O_3/SiO_2 composites fabricated using reverse-micelle and sol-gel methods. The heating process was performed at various temperatures to figure out the optimal conditions for acquisition of the ε-Fe_2O_3 phase, which exhibits the largest coercive field among the Fe oxides. The sample treated at 1,075 °C had the highest percentage of ε-Fe_2O_3 phase, with a coercivity (H_C) of 21.57 kOe measured at room temperature that reached a maximum of 23.7 kOe at 230 K. The measurement of the magnetization-temperature (M-T) curve for this sample also reveals the characteristic magnetic transition associated with ε-Fe_2O_3 within the temperature range of 40-150 K. The crystal structure of ε-Fe_2O_3 was confirmed using X-ray powder diffraction. Transmission electron micrographs revealed a broad size distribution of iron oxide nanoparticles ranging from 12 to 22 nm. The findings indicate that ε-Fe_2O_3 is a promising candidate with high electromagnetic-wave absorption capacity that is appropriate for high-speed wireless communication applications.

Keywords : ε-Fe_2O_3, reverse-micelle and sol-gel method, heat-treatment, coercivity

1. Introduction

Magnetic iron oxide-based nanoparticles have received considerable attention for specific applications [1-3]. Iron oxides are used in technological applications, such as permanent magnets, magnetic recording, and information storage [4, 5], as well as biomedical applications, including magnetic fluids, magnetofection, cancer therapy, and drug delivery [6-8]. They are also crucial to theoretical studies that examine the quantum tunneling of magnetization and the impact of interparticle magnetic interactions on a nanoparticle system's magnetic regime [9, 10]. There are three naturally occurring iron oxides: Fe(II) oxide (FeO), Fe(III) oxide (Fe_2O_3), and Fe_3O_4 (compound of Fe(II)-oxide and Fe(III)-oxide).

Iron (III) oxide exists as four polymorphs: α-Fe_2O_3 (hematite), β-Fe_2O_3, γ-Fe_2O_3 (maghemite), and ε-Fe_2O_3; each polymorph has a distinct structure and properties [4, 11, 12]. Among these four polymorphs, α-Fe_2O_3 and γ-Fe_2O_3, which occur in both bulk and nanosized forms, are commonly found in nature and have been widely investigated. α-Fe_2O_3 is a red-brown solid with corundum structure that exhibits excellent properties, including low cost, abundant availability, wide light absorption, environment compatibility, and thermal stability [2, 13, 14]. Accordingly, α-Fe_2O_3 is appropriate for many applications in catalysis [15], biomedicine and biotechnology [16], gas sensors [17], and rechargeable lithium-ion batteries [18, 19]. γ-Fe_2O_3 has a cubic spinel structure and exhibits ferromagnetic ordering with a net magnetic moment (2.5 μ_B per formula unit) and high Neel temperature (~950 K). Additionally, its chemical stability and low cost enables wide application in magnetic recording devices, electromagnetic absorbers, and biomedical engineering [20-22]. In contrast, β-Fe_2O_3 and ε-Fe_2O_3 are rare phases with low natural abundances. It is challenging to synthesize them as a single phase because they only exist as nanosized

*Co-corresponding author: Tel: +82-42-821-6633
Fax: +82-42-822-3206, e-mail: jrjeong@cnu.ac.kr
e-mail: hyojkim@cnu.ac.kr
†These authors contributed equally to this work

structures and are thermally unstable; they readily transform into the α-phase. Notably, ε-Fe_2O_3, which appears as an intermediate phase between α-Fe_2O_3 and γ-Fe_2O_3, has an extremely large magnetic coercive field of 20 kOe at room temperature [23]. Furthermore, it exhibits electromagnetic-wave absorption with a high resonance frequency, which can be used in information storage, magnetic-field tunable devices, and magnetic recording media [23-25]. The physical aspects of the ε-Fe_2O_3 phase are poorly understood [26-29]. Many chemical and physical methods have been used to prepare high-percentage ε-Fe_2O_3-phase samples; for example, chemical vapor decomposition [30], flame spray pyrolysis [31], spray drying method [32], sol-gel method [33], pulsed laser deposition [34], sputtering [35], and thermal decomposition [36, 37].

Here, we report the synthesis of high percentage of ε-Fe_2O_3/SiO_2 nanoparticles by combining the reverse-micelle and sol-gel methods. The reverse micelle process offers distinct advantages over alternative methodologies, notably enhanced precision in regulating particle dimensions, shapes, uniformity, and dispersal. In addition, the sol-gel process affords superior control over composition, primarily due to the silica matrix's role in inhibiting the agglomeration and phase transition of ε-Fe_2O_3 particles into α-Fe_2O_3. During the reverse micelle procedure, the precursor $Fe(OH)_3$ was uniformly produced and well dispersed. The hydrolysis occurs slowly and homogenously in the sol-gel procedure. This combination method created favorable conditions for the formation of ε-Fe_2O_3 particles in the range of several tens nanometers in size. We investigated the formation and stability of the ε-Fe_2O_3 phase in the temperature range between 700 °C and 1,300 °C. These measurements established a maximal coercivity (H_C) of ~21.57 kOe for the sample heated at 1,075 °C, which was identified as the optimal treatment temperature to obtain ε-Fe_2O_3. The temperature dependence of H_C was also investigated.

2. Experimental

Figure 1 schematically illustrates the synthetic route to ε-Fe_2O_3 nanoparticles. In the reverse-micelle step, two types of reverse-micelle systems were prepared: R-micelle A and B. With stirring, the two reverse-micelle solutions were prepared from the 0.03/0.12/0.33/1 molar ratio of cetyltrimethylammonium bromide/1-butanol/n-octane/H_2O. To R-micelle A, 0.74 mmol of $Fe(NO_3)_3$ was added to obtain a yellow solution (R-A); to R-micelle B, 30 mmol of NH_3 was dissolved to obtain the R-B solution. The R-B solution was added dropwise into the R-A solution while stirring for 30 min to obtain a brown solution. Then, 6.7 mmol of tetraethoxysilane was slowly injected into the brown solution. Stirring was maintained for 24 h at room temperature, producing a yellow-brown solution. The obtained precipitate was collected by centrifugation, washed several times with $CHCl_3$ and CH_3OH, and dried. Then, the dry powder was heated at 700 °C, 975 °C, 1,000 °C, 1,025 °C, 1,050 °C, 1,075 °C, 1,150 °C, or 1,300 °C for 4 h to obtain a series of samples.

The crystallinity of each sample was confirmed using high-resolution X-ray diffraction (XRD; Bruker D8; Bruker Corp., Billerica, MA, USA). The magnetic properties of the samples were evaluated using a vibrating sample magnetometer (model 7304; Lake Shore Cryotronics, Inc., Westerville, OH, USA) and a Quantum Design physical property measurement system (Evercool II-9T;

Fig. 1. (Color online) Schematic illustration of the synthesis of the ε-Fe_2O_3 phase.

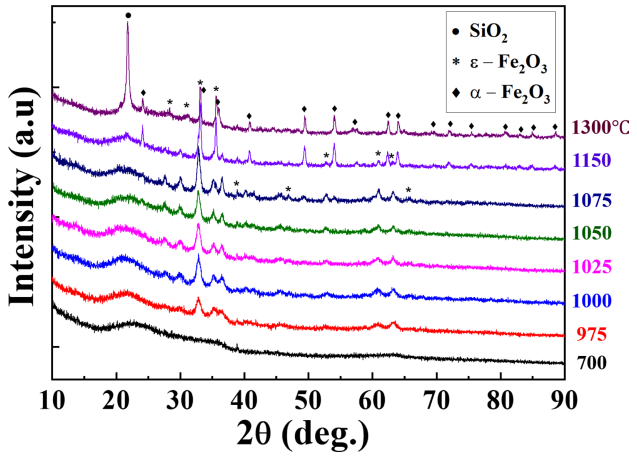

Fig. 2. (Color online) X-ray diffraction patterns of samples heated at different temperatures.

Quantum Design, Inc., USA). The morphologies of the samples were examined by transmission electron microscopy (TEM; JEM 2010; JEOL Ltd.).

3. Results and Discussion

Figure 2 presents the XRD patterns of the samples heated at different temperatures. When heating at a low temperature (700 °C), there was only a broad peak near 21.7°, which was attributed to amorphous SiO_2. Iron oxide phases formed with increasing temperature. Up to 1,075 °C, the many peaks observed were matched to ε-Fe_2O_3 signature XRD peaks. The remaining several peaks with extremely low intensity that corresponded to the α-Fe_2O_3 phase indicated that the sample was not composed of 100 % ε-Fe_2O_3 phase. This result has been frequently reported in other studies because the ε-Fe_2O_3 phase is thermally unstable [29, 38, 39]. An increasing temperature caused the intensity of the α-Fe_2O_3 peaks to significantly increase, indicating that the portion of α-Fe_2O_3 was increasing. The crystallite size of the ε-Fe_2O_3 nanoparticles was estimated from the full-width at half-maximum (FWHM) of the peak centered at 2θ = 32.93° according to the Debye–Scherrer's equation, as follows:

$$D = \frac{k\lambda}{\beta\cos\theta}$$

where k is the particle geometry-dependent constant, λ is the X-ray wavelength (1.5406 Å), β is the FWHM of the peak, and θ is the diffracted angle. Here, the particle size of 1,075 °C-sample was estimated to be 16.78 nm.

The sizes and shapes of the Fe_2O_3 particles were additionally investigated by TEM for the sample heated at

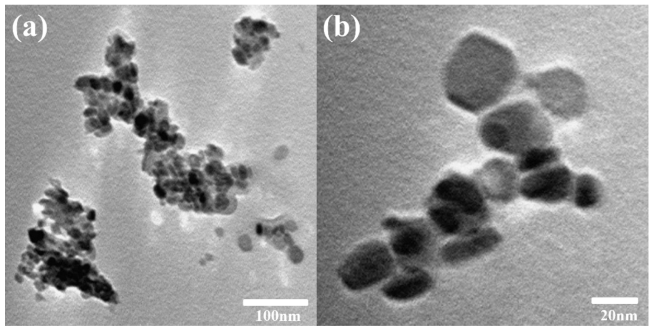

Fig. 3. (a) low-magnification and (b) high-magnification transmission electron micrographs of Fe_2O_3 nanoparticles heated at 1,075 °C.

1,075 °C, which had the largest percentage of the epsilon phase. Silica matrices were etched by stirring in an aqueous sodium hydroxide solution at 70 °C for 24 hours. The phase ratio of the sample heated at 1,075 °C obtained using the reference intensity ratio method was 96.2 % ε-Fe_2O_3 and 3.8 % α-Fe_2O_3. The TEM images (Fig. 3) revealed spherical particles and a highly uniform particle size distribution ranging from 12 to 22 nm, with a mean size of 17 ± 1 nm. This size range is favorable for maintenance of the ε-Fe_2O_3 phase because it converts to the α-Fe_2O_3 phase if the particle size exceeds ~30 nm [12, 31]. The particle size observed by TEM was in good agreement with the size determined by XRD.

One of the signature magnetic properties of the ε-Fe_2O_3 phase is its large H_C, which can be used as a unique criterion to determine whether the ε-Fe_2O_3 phase exists in composite nanoparticles. Field-swept vibrating sample magnetometry measurement at room temperature was performed to obtain magnetic hysteresis loops of the samples, which revealed the field dependence of magnetization curves for samples heated at different temperatures. The sharp decrease at ~3,000 Oe indicated the presence of a minor amount of α-Fe_2O_3, which was an impurity in the ε-Fe_2O_3 phase. The H_C of samples increased with increasing heating temperature and reached a maximum at 1,075 °C. However, the signal of the α-Fe_2O_3 phase in the hysteresis loop persisted. A further increase in temperature reduced the H_C. This behavior is in good agreement with the XRD result, indicating that the evolution of ε-Fe_2O_3 and α-Fe_2O_3 is a function of temperature and the coexistence of two phases within a particular temperature range. According to the measurement, the highest H_C of ~21.57 kOe was achieved for the sample heated at 1,075 °C. To clearly visualize the change in H_C, its amplitude was plotted as a function of heating temperature (Fig. 4(b)).

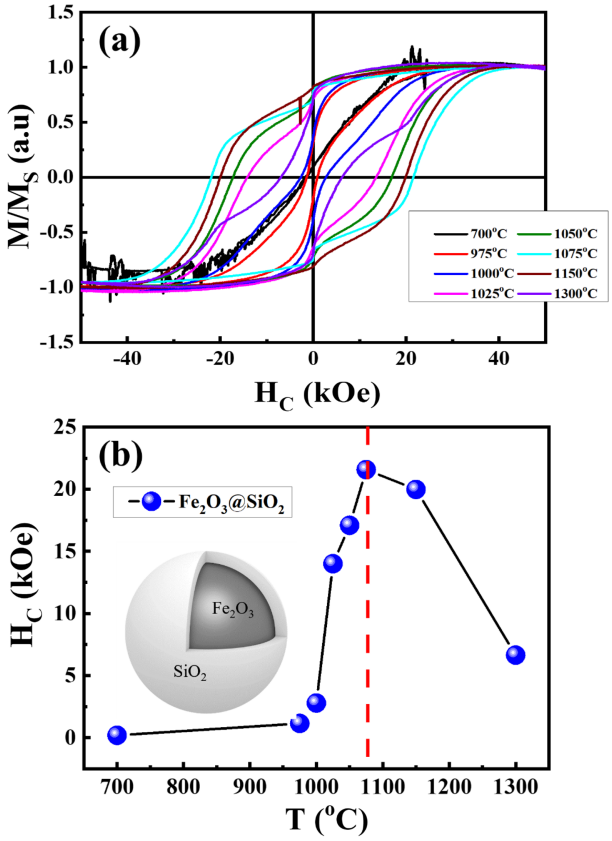

Fig. 4. (Color online) (a) Normalized magnetization versus magnetic-field curve for various heating temperatures of samples at 300 K. (b) Coercivity as a function of heating temperature. Inset illustrates Fe_2O_3/SiO_2 nanoparticles.

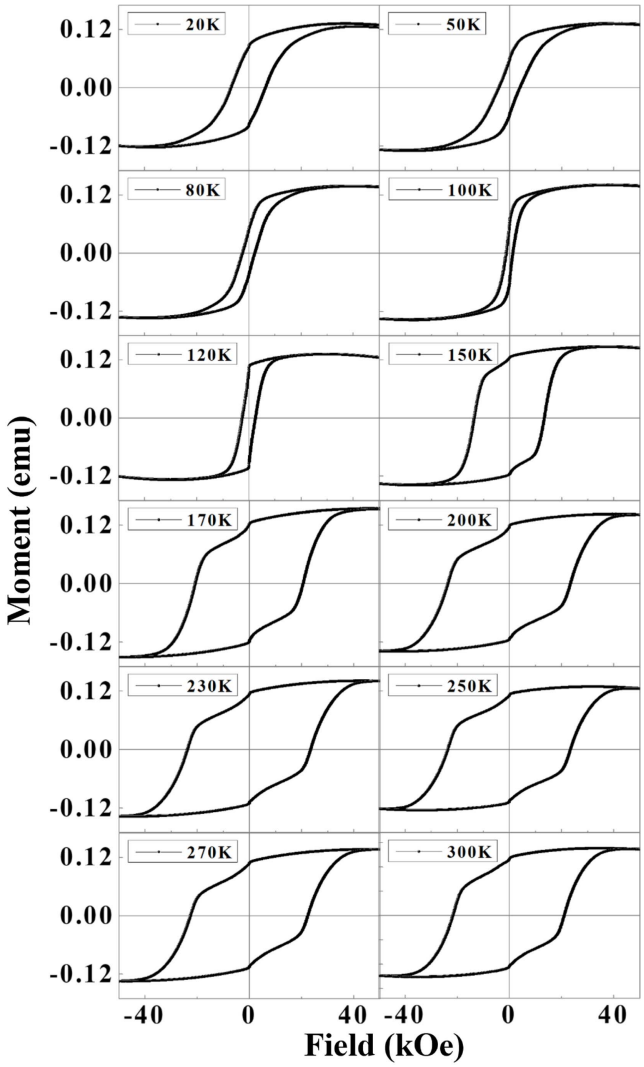

Fig. 5. Magnetic hysteresis loops of the sample heated at 1,075 °C measured at different temperatures.

The hysteresis loops of the sample heated at 1,075 °C were measured at 20, 50, 80, 100, 120, 150, 180, 200, 230, 250, 270, and 300 K in a full magnetic-field scan from –50 to 50 kOe. These loops revealed the temperature dependence of the magnetic properties (Fig. 5). As noted above, this sample continued to include some α-Fe_2O_3; thus, the loops were a combination signal of α-Fe_2O_3 and ε-Fe_2O_3 phases. However, below 150 K, α-Fe_2O_3 is a weak ferromagnet; beyond this temperature, it is superparamagnetic, indicating that the H_C of α-Fe_2O_3 shows negligible variation according to temperature. For that reason, the change in H_C was mostly related to the contribution of the ε-Fe_2O_3. The temperature dependency of H_C is clearly shown in Fig. 6(a). The coercive field slightly increased with decreasing temperature, reaching a maximum value of 23.7 kOe at 230 K. However, a sharp decrease in H_C was observed between 170 K and 100 K, with the lowest H_C of 1.3 kOe occurring at 100 K. Additionally, H_C slightly increased upon further cooling to 20 K, reaching a value of 6.7 kOe. This behavior was attributed to increasing anisotropy, which is most likely related to the dominance of surface anisotropy at low temperatures [40]. The abrupt decrease in H_C measured at 100 K also confirmed the presence of ε-Fe_2O_3; this phenomenon originated from the magnetic phase transition, which led to a decrease in H_C. The magnetic moment as a function of temperature is presented in Fig. 6(b). The zero-field cooling curve under 50 kOe increased at 41 K, achieving its maximum value at ~149 K, which constitutes behavior characteristic of the ε-Fe_2O_3 phase.

4. Conclusion

High-concentration (~96.2 %) ε-Fe_2O_3 nanoparticles were synthesized via combined reverse-micelle and sol-gel methods. The structure properties of 1,075 °C-sample has been studied by XRD and TEM. These measurements

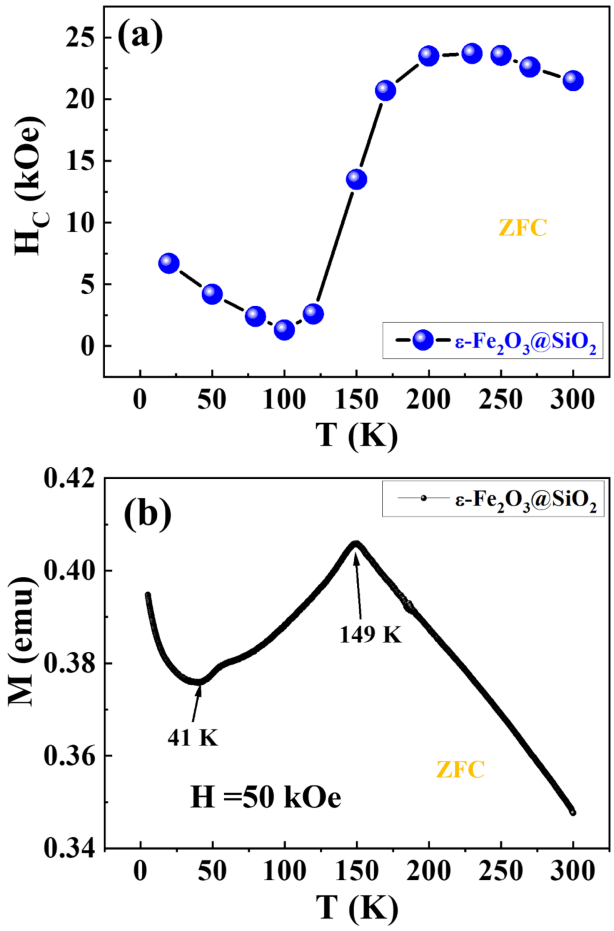

Fig. 6. (Color online) (a) Coercivity as a function of measurement temperature for the sample heated at 1,075 °C. (b) Zero-field cooling curve of the same sample measured at 50 kOe.

revealed roughly spherical nanoparticles with a mean size of ~17 nm. A substantial coercivity (H_C) of 21.57 kOe and 23.7 kOe was observed at temperatures of 300 K and 230 K, respectively, for the sample subjected to heating at 1,075 °C. Based on the temperature dependence of the magnetic moment, a magnetic transition typical of ε-Fe_2O_3 was observed in the range of 40-150 K.

Acknowledgments

This work was supported by the Chungnam National University.

References

[1] R. H. Kodama, J. Magn. Magn. Mater. **200**, 359 (1999).
[2] A. S. Teja and P. Y. Koh, Prog. Cryst. Growth Charact. Mater. **55**, 22 (2009).
[3] W. Wu, Q. He, and C. Jiang, Nanoscale Res. Lett. **3**, 397 (2008).
[4] Dr. R. M. Cornell, Prof. em. Dr., Dr. h.c. U. Schwertmann, Wiley-VCH: Weinheim, Germany, (2003).
[5] M. L. Plumer, J. Ek, and D. Weller, Springer, Berlin (2001).
[6] K. Raj and R. Moskowitz, J. Magn. Magn. Mater. **85**, 233 (1990).
[7] S. Mornet, S. Vasseur, F. Grasset, and E. Duguet, J. Mater. Chem. **14**, 2161 (2004).
[8] A. Ito, M. Shinkai, H. Honda, and T. Kobayashi, J. Biosci. Bioeng. **100**, 1 (2005).
[9] W. Xue, Z. C. Wang, S. G. He, Y. Xie, and E. R. Bernstein, J. Am. Chem. Soc. **130**, 15879 (2008).
[10] E. N. Zare, T. Abdollahi, and A. Motahari, Arab. J. Chem. **13**, 2331 (2020).
[11] R. Zboril, M. Mashlan, and D. Petridis, Chem. Mater. **14**, 969 (2002).
[12] J. Tuček, R. Zbořil, A. Namai, and S. I. Ohkoshi, Chem. Mater. **22**, 6483 (2010).
[13] L. Pauling and S. B. Hendricks, J. Am. Chem. Soc. **47**, 781 (1925).
[14] J. Wu, S. Mao, Z. G. Ye, Z. Xie, and L. Zheng, ACS Appl. Mater. Interfaces. **2**, 1561 (2010).
[15] F. Shi, M. K. Tse, M. M. Pohl, A. Brückner, S. Zhang, and M. Beller, Angew. Chem. Int. Ed. Engl. **46**, 8866 (2007).
[16] H. Zangeneh, A. A. L. Zinatizadeh, M. Habibi, M. Akia, and M. Hasnain Isa, J. Ind. Eng. Chem. **26**, 1 (2015).
[17] A. Mirzaei, S. G. Leonardi, and G. Neri, Ceram. Int. **42**, 15119 (2016).
[18] L. Xu, Y. Tian, T. Liu, H. Li, J. Qiu, S. Li, H. Li, S. Yuan, and S. Zhang, Green Ener. & Env. **3**, 156 (2018).
[19] L. Ji, O. Toprakci, M. Alcoutlabi, Y. Yao, Y. Li, S. Zhang, B. Guo, Z. Lin, and X. Zhang, ACS Appl. Mater. Interfaces. **4**, 2672 (2012).
[20] R. Dronskowski, Adv. Funct. Mater. **11**, 27 (2001).
[21] Z. Xiang, B. Deng, C. Huang, Z. Liu, Y. Song, and W. Lu, J. Alloys Compd. **822**, 153570 (2020).
[22] M. Lévy, C. Wilhelm, J. M. Siaugue, O. Horner, J. C. Bacri, and F. Gazeau, J. Phys. Condens. Matter. **20**, 204133 (2008).
[23] J. Jin, S. I. Ohkoshi, and K. Hashimoto, Adv. Mater. **16**, 48 (2004).
[24] A. Namai, M. Yoshikiyo, K. Yamada, S. Sakurai, T. Goto, T. Yoshida, T. Miyazaki, M. Nakajima, T. Suemoto, H. Tokoro, and S. I. Ohkoshi, Nat. Commun. **3**, 1035 (2012).
[25] M. Yoshikiyo, A. Namai, and S. Ohkoshi, J. Jpn. Soc. Powder and Powder Metallurgy. **61**, S280 (2014).
[26] L. Machala, J. Tuček, and R. Zbořil, Chem. Mater. **23**, 3255 (2011).
[27] A. I. Dmitriev, O. v. Koplak, and R. B. Morgunov, J. Surf. Investig. **9**, 442 (2015).
[28] M. Gich, I. Fina, A. Morelli, F. Sánchez, M. Alexe, J. Gàzquez, J. Fontcuberta, and A. Roig, Adv. Mater. **26**, 4645 (2014).

[29] J. Kohout, P. Brázda, K. Závěta, D. Kubániová, T. Kmječ, L. Kubíčková, M. Klementová, E. Šantavá, and A. Lančok, J. Appl. Phys. **117**, 17D505 (2015).
[30] D. Barreca, G. Carraro, D. Peeters, A. Gasparotto, C. Maccato, W. M. M. Kessels, V. Longo, F. Rossi, E. Bontempi, C. Sada, and A. Devi, Chem. Vap. Depos. **20**, 313 (2014).
[31] S. Lee and H. Xu, J. Phys. Chem. C. **120**, 13316 (2016).
[32] G. R. Jo, M. B. Yun, Y. H. Son, B. Park, J. G. Lee, Y. G. Kim, Y. G. Son, and Y. K. Baek, Chem. Commun. **58**, 11442 (2022).
[33] M. Popovici, M. Gich, D. Nižňanský, A. Roig, C. Savii, L. Casas, E. Molins, K. Zaveta, C. Enache, J. Sort, S. de Brion, G. Chouteau, and J. Nogués, Chem. Mater. **16**, 5542 (2004).
[34] M. Watanabe, J. Nanosci. Nanotechnol. **16**, 2509 (2016).
[35] S. Chen, Y. Jiang, T. Yao, A. Tao, X. Yan, F. Liu, C. Chen, X. Ma, and H. Ye, Micron, **163**, 103359 (2022).
[36] K. Kelm, W. Mader, and Z. Anorg, Allg. Chem. **631**, 2383 (2005).
[37] R. Zboril, M. Mashlan, K. Barcova, and M. Vujtek, Hyperfine Interact. **139**, 597 (2002).
[38] J. Ma and K. Chen, Ceram. Int. **44**, 19338 (2018).
[39] A. Namai, M. Yoshikiyo, S. Umeda, T. Yoshida, T. Miyazaki, M. Nakajima, K. Yamaguchi, T. Suemoto, and S. I. Ohkoshi, J. Mater. Chem. C. Mater. **1**, 5200 (2013).
[40] M. Gich, A. Roig, C. Frontera, E. Molins, J. Sort, M. Popovici, G. Chouteau, D. Martín y Marero, and J. Nogús, J. Appl. Phys. **98**, 044307 (2005).